# Thermal and mechanical performance of a novel 3D printed macro-encapsulation method for phase change materials

**Marcus Maier[1,*], Brian Salazar[2], Cise Unluer[4], Hayden K. Taylor[2], Claudia P. Ostertag[3],**

[1]Berkeley Education Alliance for Research in Singapore (BEARS)

[2]Department of Mechanical Engineering, University of California, Berkeley, Berkeley, CA, USA

[3]Department of Civil and Environmental Engineering, University of California, Berkeley, Berkeley, CA, USA

[4] School of Engineering, University of Glasgow, G12 8LT, Glasgow, United Kingdom

## Abstract

The mechanical and thermal properties of a novel 3D-printed macro-encapsulation method for Phase Change Materials (PCMs) was investigated and compared to mixtures that contain commercially available micro-encapsulated PCMs. Two types of cement-based mixtures, a mortar mix with a density of 2,161 kg/m$^3$ and a lightweight mix with a density of 1,351 kg/m$^3$, were utilized for both the micro- and macro-encapsulated samples. The micro-encapsulated mortar and lightweight samples contain 0 vol%, 10 vol%, and 20 vol% of PCMs with a melting point of 28 °C. The macro-encapsulated samples contain 20 vol% of the same PCMs but in this case the PCMs were incorporated into a hollow 3D-printed polymer lattice which is embedded in the cement-based matrices. This lattice not only serves as macro-encapsulation but also as reinforcement to enhance the ductility of cement-based materials. The results reviled that the lattice specimens developed the lowest panel temperature during heating and showed a significant reduction of the indoor temperature. The mechanical properties of the lattice specimens were improved and resulted in a change from a brittle to strain-hardening behavior. This research shows the potential of the developed system to be uses for thermal retrofitting or as wall elements to lower the indoor temperature and save energy in tropical climates.

Keywords: Phase Change Materials; Thermal energy storage; Cenospheres; Concrete; 3D-printing; macro-encapsulation;

## 1 Introduction

Building envelopes are designed to carry structural loads and protect people from the environmental climate including diurnal thermal changes. To address the diurnal thermal impact on a building and on people different systems have been developed to hinder the thermal exchange between the inside and outside of the building. These building envelope systems vary greatly in terms of wall design (e.g. different layer systems, insulation layers and/or ventilated facades etc.) and, therefore, in a wide range of construction effort and costs. A monolithic design of the exterior walls is a cost- and time-effective construction method and of common practice especially when cementitious materials are used. Concrete facades benefit from higher mechanical strength and low maintenance costs but, unfortunately, lack in thermal performance. This results either in high diurnal temperature change within the building or in high energy consumption for heating or cooling. For instance, in Singapore 60 % of the electricity consumption is used by air-conditioning to cool space in residential and non-residential buildings [1]. On the other hand, most of Singapore's schools are mechanically ventilated by fans and not air-conditioned which results in classroom temperatures up to 27-32 °C [2]. To address these issues, methods have been investigated to enhance the thermal performance of concrete by developing new concrete mixtures for monolithic construction. One such approach is the incorporation of Phase Change Materials (PCMs) into concrete mixtures. The melting and freezing process of PCMs

stores and releases energy within a narrow temperature range. This behavior has the potential to decrease the temperature fluctuation within a building and, therefore, save heating and cooling costs and has caught the interest of several research groups [3-15].

The majority of the PCMs consists of paraffin that are available in a wide range of melting temperatures [16-18]. But there are two major challenges when PCMs are used in cementitious mixtures - the PCMs low thermal conductivity of about 0.21 – 0.23 W/mK [19] and the leakage of the liquid paraffin phase into the cement based mixtures. Several researchers enhanced the thermal conductivity by incorporating carbon fibers or expanded graphite which promotes the heat diffusion into the paraffin [20-24]. Additional research addressed the leakage challenge by developing encapsulation methods for paraffins which range from imbuing of porous materials with PCMs to provide micro- and/or macro-encapsulation of the paraffin [25-30].

Macro-encapsulated methods are mostly referred to paraffin filled into pockets, balls or plates and are incorporated into the wall system as layers. This requires additional effort compared to monolithic designed walls [31-35]. Micro-encapsulation, one the other hand, is a method where PCM particles are covered with a thin polymeric film to avoid leakage during its phase change [5, 36-40] but this thin film lacks in mechanical strength and is therefore sensitive to damage when mixed into concrete and mortar [41, 42]. Several micro-encapsulation methods were developed to enhance the mechanical strength of the PCMs and, therefore, allow higher amounts of PCMs to be incorporated for a better thermal performance of the mixtures [4, 43-46]. For instance, Hunger et al. [43] investigated the thermal performance of cementitious materials with various volume fractions of micro-encapsulated PCMs. Their study revealed that the PCM mixture with the highest volume % (e.g. with 5% PCMs by volume) exhibited a compressive strength loss of 69%. In their research, Hunger et al. concluded that the loss of compressive strength is due to the substantial gap-difference in the intrinsic strength of the micro-encapsulated PCMs and the concrete matrix as well as due to the damage of micro-encapsulation of the PCMs during the mixing and fabrication process of the concrete members.

In this paper a novel 3-D printed macro-encapsulation method is being introduced with the aim of providing a mechanically stable and durable encapsulation method for monolithic exterior wall systems. For this purpose, a hollow 3D-printed lattice was filled with paraffin and embedded in a cement-based matrix to investigate thermal and mechanical properties of this novel system. The beneficial mechanical properties of the 3D-printed lattice reinforced system were already shown by the researchers in [47]. Focus was placed on the mechanical and thermal assessment of two cement-based mixtures, a mortar mixture and a lightweight mixture. The developed system has the potential to be used as a monolithic exterior wall system with improved thermal performance or as panel elements to retrofit existing buildings with the aim to lower the electricity consumption and indoor temperature for buildings in tropical climates.

## 2 Materials and Methods

### 2.1 Materials

Two mixtures were prepared, an ordinary mortar mixture with fine sand and a lightweight mixture with cenospheres instead of sand aggregates. Ordinary Portland cement, CEM I, according to Singapore Standard SS EN 197-1 was used for both the mortar and lightweight mixtures. The composition of the cement is listed in Table 1.

Table 1 Composition of CEM I

| Composition | Cem I [%] |
|---|---|
| $SiO_2$ | 20-25 |
| $Al_2O_3$ | 5-6 |
| $Fe_2O_3$ | 2-3 |
| CaO | 60-65 |
| MgO | 1-2 |
| $Na_2O$ | 0.2-0.3 |
| $K_2O$ | 0.4-0.5 |
| Free lime as CaO | 0.5-1.0 |
| $C_3A$ | 5-10 |

Fine sand with a maximum grain size of 2 mm and a fineness modulus of 3.2 was used for the mortar mixtures. The grain size distribution of the fine sand is shown in Figure 1.

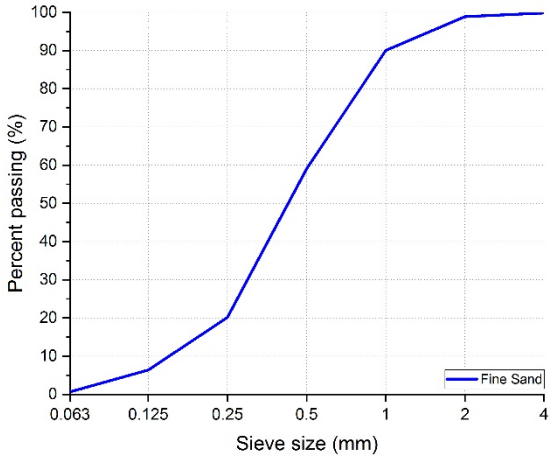


Figure 1: Sieve curve of the fine aggregates

For the lightweight mixtures, silica fume and cenospheres which are lightweight, hollow spheres made largely of silica and alumina were utilized. The properties of the cenospheres are given in Table 2.

Table 2 Technical Data of Cenospheres

| Cenosphere QK300 | |
|---|---|
| True Density [kg/m³] | 850 |
| Bulk Density [kg/m³] | 450 |
| Crush Strength [MPa] | 17.2 |
| Size range [µm] | 45-300 |
| Particle size D10 [microns][1] | 75 |
| Particle size D50 [microns][1] | 180 |
| Particle size D90 [microns][1] | 275 |
| Therm. conductivity [W/mK] | 0.18 |
| Melting point [°C] | 1300 |

| | |
|---|---|
| Softening point [°C] | 1250 |
| Moisture rate [%] | <0.5% |
| pH-Value [-] | 7-8 |

[1]10% (D10) and 90% (D90) of the particles are smaller than 75 and 275 microns respectively. D50, 50% of the particles are smaller than 180 microns. D50 represents the median diameter

A polycarboxylate ether-based superplasticizer was used for the lightweight mixtures. A micro-encapsulated paraffin with a melting point of 28 °C and particle size in the range of 15 to 30 microns was incorporated into both cement-based mixtures. In comparison, pure paraffin wax with the same melting temperature was used for the novel encapsulation method introduced in this research. All PCMs were obtained from the same manufacturer. The selection of a phase change temperature of 28 °C was to ensure that the PCM can be fully discharged during the night in Singapore as confirmed by research in [48].

## 2.2 Mix proportion

Both the mortar mixtures and the cenosphere mixtures contain 0, 10% and 20% of PCMs by volume. All mortar mixtures have a water-to-cement ratio of 0.5 and contain sand as fine aggregates. The control mixture contains 52.8 vol% of sand and the sand was then partially replaced by PCMs according to their volume fractions. The lightweight mixtures consist of cement, silica fume, and cenospheres with a water-to-cement ratio of 0.36 resulting in 40.6 vol% of cenospheres for the control mixture. The cenospheres were partially replaces by the PCMs according to their volume fractions. Additionally, the mixtures with 0 vol% of PCMs served as matrices for the 3D-printed hollow lattice encapsulation. The hollow octet lattice, 3D-printed with ABS, is shown in Figure 2**.** The lattice was filled with pure PCM-paraffin. The selected lattice geometry was able to contain 20 vol% of paraffin by volume of concrete resulting in an overall volume, PCM plus ABS lattice, of 37%. Table 3 and Table 4 show the composition of the mortar and the cenosphere mixtures, respectively. The notation used in the following are xxP28 where the xx represent the volume percentage of the incorporated microencapsulated PCMs and P28 the melting point of the phase change materials. M represents mortar specimens whereas C represents cenosphere samples, therefore C20P28 represents a cenosphere mix with 20 vol% of PCMs.

To reduce the damage to the micro-encapsulated PCMs, the dry constituents of the mortar mixture were first stirred for 90 seconds to ensure a well-mixed blend. The PCMs were then added and stirred for 60 seconds, followed by water addition and 3 minutes of mixing.

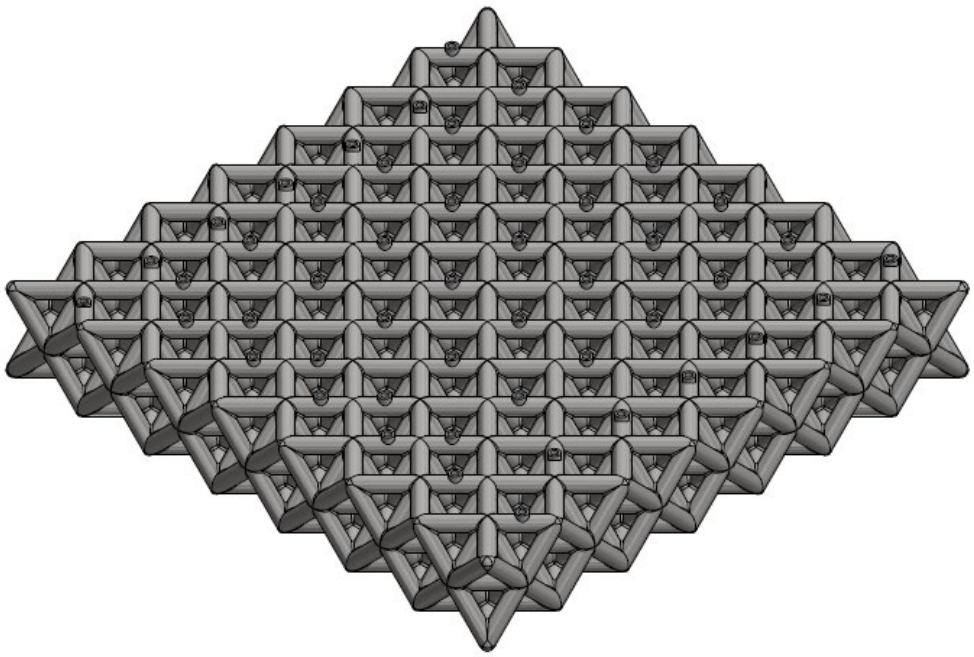

Figure 2: 3D-printed octet lattice that serves both as encapsulation for the PCMs and as matrix reinforcement.

Table 3: Composition of the mortar mixture with varying amount of PCMs

| Batch notation Mortar | Density | Mortar Control mixture | M10P28 10 Vol % PCM-28 | M20P28 20 Vol % PCM-28 | Mortar Lattice mixture |
|---|---|---|---|---|---|
| Cement: CEM I [kg/m³] | 3100 | 550 | 550 | 550 | 550 |
| Sand: 0-2 mm [kg/m³] | 2700 | 1424 | 1155 | 885 | 1424 |
| Water [kg/m³] | 1000 | 275 | 275 | 275 | 275 |
| PCM - 28 °C [kg/m³] | 900 | -- | 90 | 180 | -- |
| W/B ratio [-] | -- | 0.50 | 0.50 | 0.50 | 0.50 |
| SP-ACE8538 [% of CEM] | -- | 0.10 | 0.29 | 1.16 | 0.10 |
| Flow table test [mm] | -- | 130 | 140 | 125 | 130 |

Table 4: Composition of the lightweight mixture with varying amount of PCMs

| Batch notation Cenospheres | Density | Ceno-Control mixture | C10P28 10 Vol % PCM-28 | C20P28 20 Vol % PCM-28 | Ceno Lattice mixture |
|---|---|---|---|---|---|
| Cement: CEM I [kg/m³] | 3100 | 775 | 775 | 775 | 775 |
| Silica Fume [kg/m³] | 2200 | 67 | 67 | 67 | 67 |
| Cenospheres [kg/m³] | 850 | 325 | 245 | 165 | 325 |
| Water [kg/m³] | 1000 | 303 | 303 | 303 | 303 |
| PCM - 28 °C [kg/m³] | 900 | -- | 90 | 180 | -- |
| W/B ratio [-] | -- | 0.36 | 0.36 | 0.36 | 0.36 |
| SP-ACE8538 [% of Binder] | -- | 0.13 | 0.26 | 0.93 | 0.13 |
| Flow table test [mm] | -- | 155 | 145 | 145 | 155 |

## 2.3 Experimental method and equipment

### 2.3.1 Mechanical characterization

The mechanical properties were evaluated by performing compression and bending tests at the age of 28 days. For compression tests, 5 cm cubes were prepared and tested with a loading rate of 55 kN/min. Four-point bending tests on beams with 50 × 50 × 300 mm were performed to evaluate the bending capacity and post cracking behavior. A loading rate of 0.2 mm/min was chosen for all tests. At least 3 samples of each mixture were prepared for each test.

### 2.3.2 Thermal performance

In addition to the mechanical characterization, the thermal properties were assessed by means of Differential Scanning Calorimetry and a so called “Hot Box” test setup.

### 2.3.3 Differential Scanning Calorimetry

Differential Scanning Calorimetry (DSC) measurements were performed on pure PCMs and on encapsulated PCMs. Pure PCMs refers here to PCMs that has been filled into the 3D printed lattice whereas the encapsulated PCMs were mixed into the cement-based matrix. The samples were tested within a temperature range of 10 to 60 °C with a heating and cooling rate of 1 °C at nitrogen atmosphere.

#### 2.3.3.1 Hot Box Test

To evaluate the thermal performance of the different mixtures and encapsulation methods, panels with dimensions of L × H × T = 30 × 30 x 5 $cm^3$ were prepared and tested with a Hot-Box setup. The Hot-Box setups, shown in Figure 3, consisted of two chambers, a reflective hollow tunnel chamber and a test chamber, separated by the test specimen as shown in Figure 4. The test specimens were heated by three radiant heat panels. The inner dimension of the two chambers is 30 x 30 x 30 $mm^3$. The walls of the chambers are made of 100 mm thick expanded polystyrene boards. In addition, the inner surfaces of the walls of the reflective hollow tunnel chamber were covered with reflective paper to ensure a uniform temperature field for the test panel. The length of the tunnel is 35 cm. Three radiant heat panels supplied the heat for the testing and were placed 15 cm in front of the tunnel. The intensity of the heat panel could be adjusted with a connected dimmer. Similar experimental setups have been used by other researchers [19, 49-53].

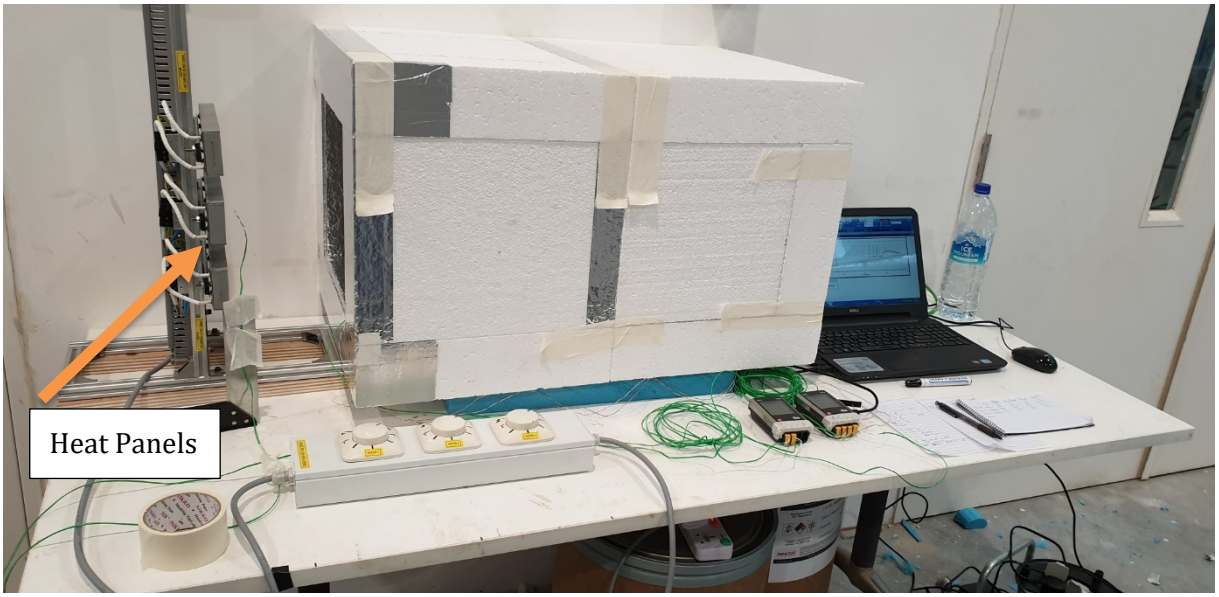


Figure 3: Hot Box test setup

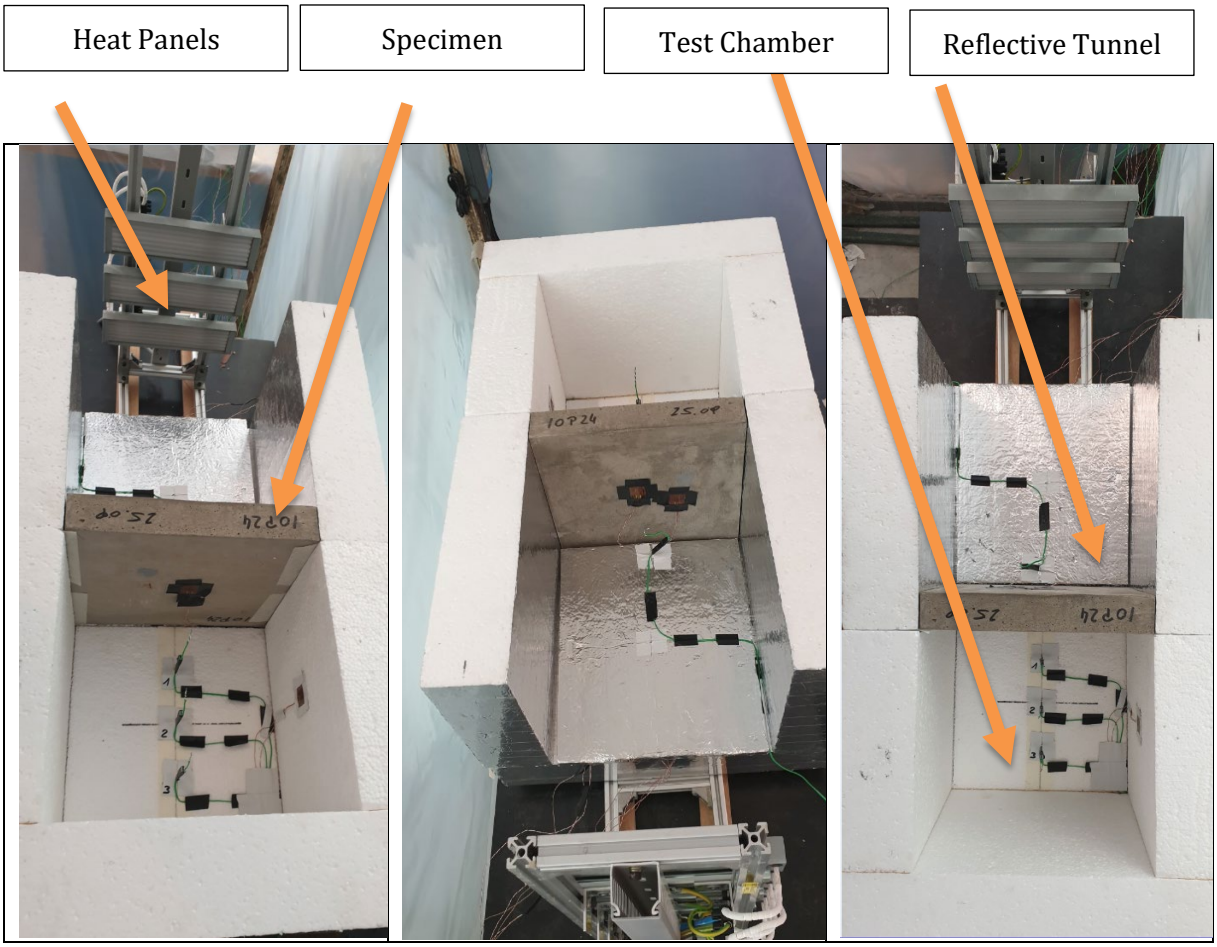


Figure 4: Hot Box test setup details

#### 2.3.3.2 Temperature and heat flux measurement

The test specimen was instrumented with four heat flux sensors and four Type K thermocouples. Two of the heat flux sensors and two thermocouples were placed on the exterior, heated surface to monitor the heat flux into the test specimen and its exterior surface temperature. The remaining two heat flux sensors and thermocouples were placed on the interior surface of the

specimen to monitor the heat flux into the test chamber as well as its interior surface temperature. The air temperature in the test chamber was recorded by three type K thermocouples at a height of 15 cm from the bottom surface and a distance of 7.5 cm, 15 cm, and 22.5 cm from the test specimen. In addition to that, the air temperature in the reflective tunnel was measured at a 2 cm distance from the heated surface of the test specimen.

#### 2.3.3.3 Thermal loading

The test duration was chosen to be 180 minutes. Each test specimen was heated for 90 min which was followed by natural cooling of 90 minutes. The heat flux into the different specimens was regulated for the first 10 minutes of testing by adjusting the radiant heat panels. This ensured a constant heat flux of approx. 500 W/m² after 10 minutes for each specimen (see Figure 5). The radiant heat of 500 W/m² is close to the mean daily solar irradiance of Singapore and was also used by several researchers in [48-50].

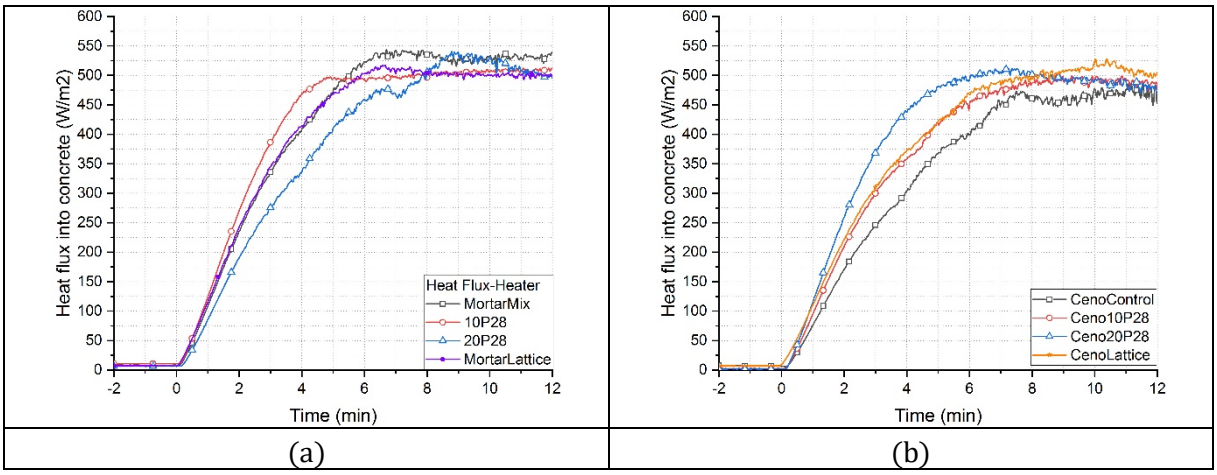


Figure 5: Cumulative Heat flux density applied to each test specimen, a) Mortar mixture, b) Cenosphere mixtures

## 3 Results

### 3.1 Mechanical and physical properties

#### 3.1.1 Density

The density of the mortar and lightweight mixtures are shown in Figure 6a, whereas the change in density, referring to the control mixes without PCMs, is shown in Figure 6b. The density was measured at an age of 7 weeks after storage of the samples for 28 days in a high humidity environment (90-98 % rel. humidity) followed by 3 weeks of laboratory storage at about 24 °C and approx. 70% rel. humidity. The density of the mortar control mixture is 2,161 kg/m³ and decreases with increasing PCM content due to the difference in density of aggregates (2,700 kg/m³) and PCMs (900 kg/m³). The lightweight mixture shows a density of 1,351 kg/m³ for the control mixture and no significant change in density is measurable with increasing PCM content due to the similar densities of PCMs (900 kg/m³) and cenospheres (850 kg/m³). The lowest density is observed for the specimens with the incorporated lattice which exhibits 1,778 kg/m³ and 1,197 kg/m³ for the mortar-lattice and cenosphere-lattice mixture, respectively.

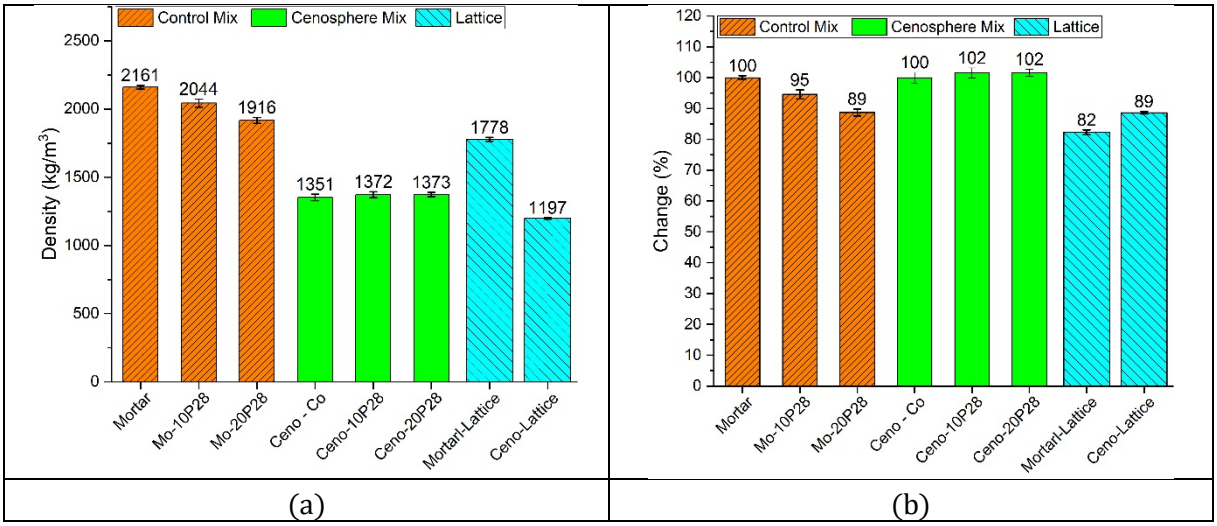


231 Figure 6: Density of mortar and lightweight mixture with 0 vol% (control mixes), 10 vol%, 20
232 vol% of PCM and the lattice specimens, a) density in kg/m³, b) change of density compared to
233 the mortar control and cenosphere control mixes in %.
234

235 ### 3.1.2 Compressive strength

236 The compressive strength of the mixtures at 28 days and the change in strength compared to the
237 control samples is given in Figure 7a and 7b, respectively. The mortar control mixture shows an
238 average compressive strength of 52.5 MPa and this strength decreases with increasing PCM
239 content (see Figure 7a). The addition of 10 vol% of PCMs to the mortar mixture reduces the
240 compressive strength to 28.2 MPa. A 20 vol% of PCMs results in a compressive strength of 16.1
241 MPa. The mixture with the incorporated lattices exhibited a compressive strength of 15.4 MPa.
242 The cenosphere control mix shows a compressive strength of 46.9 MPa and the addition of PCMs
243 has significant lower impact on the compressive strength compared to the mortar mixture (see
244 Figure 7a). The addition of 10 vol% of PCM reduces the compressive strength to 36.6 MPa, 20
245 vol% of PCMs results in a compressive strength of 33.4 MPa. The specimens with PCM-filled
246 lattices exhibited a compressive strength of 11.1 MPa. It should be noted that the 3D printed lattice
247 with the incorporated PCMs results in an overall volume of 37% of the cubes geometry. This
248 results in 17% lower concrete matrix compared to cubes containing 20 vol% of micro-
249 encapsulated PCMs and therefore to the lower compressive strength. New evolving techniques
250 will allow stronger materials to be used to fabricate these lattices and therefore can improve the
251 strength of the samples. Furthermore, an optimization of the lattice geometry has the potential to
252 improve the bulk strength.
253

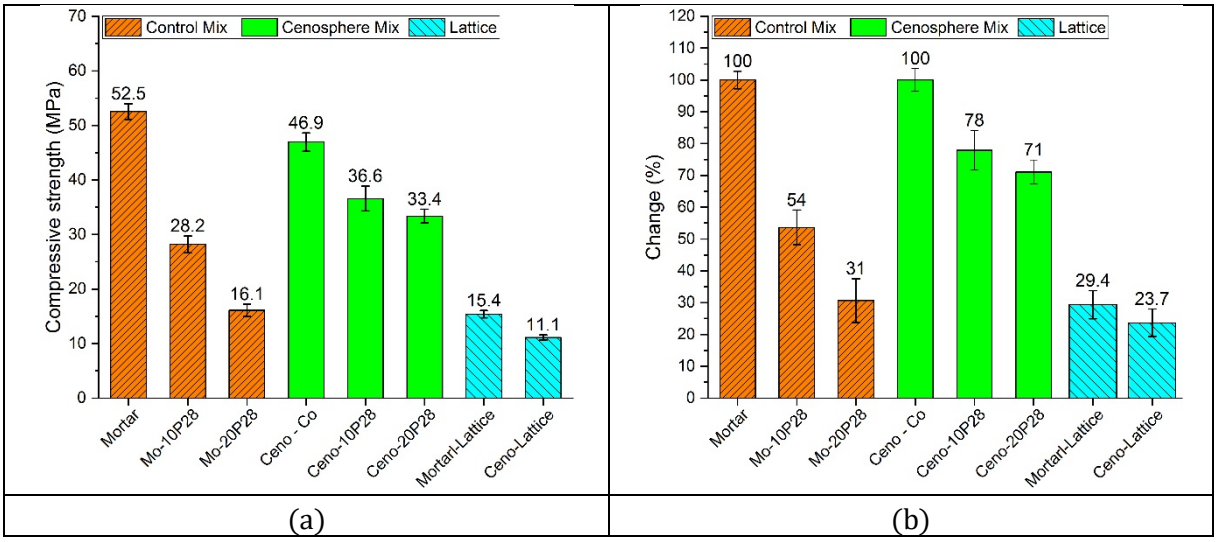


Figure 7: Compressive strength of mortar and lightweight mixture with 0 vol% (control mixes), 10 vol%, 20 vol% of PCMs and the lattices specimens a) compressive strength in MPa, b) change of compressive strength compared to the mortar and cenosphere control mixes in %.

### 3.1.3 Flexural strength

The load-deflection curves of the specimens with and without PCMs are given in Figure 8. Three specimens were tested for each mixture and PCM content. The control samples and the samples with 10 vol% and 20 vol% of PCMs showed a linear elastic behavior up to the peak load followed by an abrupt brittle failure as shown in Figure 8a and 8b. These figures include the results of all three tested samples per mix and the overlapping of the results up to failure revealed their similar elastic behavior of the control samples and the micro-encapsulated samples. Regarding the lattice samples, all specimens revealed the same behavior up to the crack initiation load but then vary in their post cracking behavior. Additionally, the specimens with the incorporated lattices revealed strain-hardening behavior followed by a smooth post cracking behavior. The most pronounced strain-hardening behavior was observed by the cenosphere lattice samples as shown in Figure 8b. Hence, the lattice reinforcement is very effective in rendering the brittle cement-based samples into quasi-brittle materials.

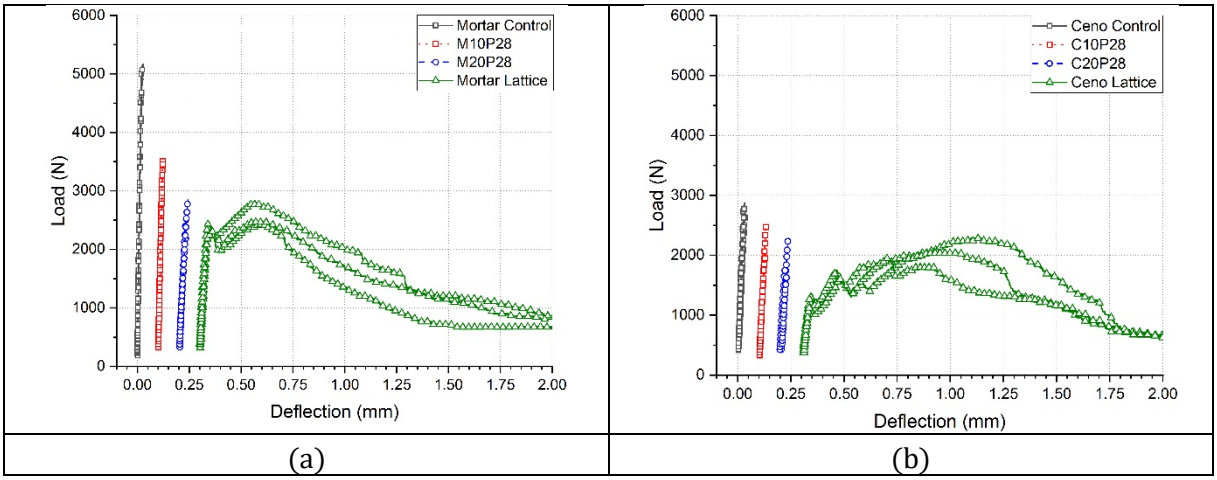


Figure 8: Load deflection curve of a) Mortar samples, b) Cenosphere samples

The peak strength was calculated by the following expression.

$$\sigma = F_{max} L / (b h^2) \quad (1)$$

where $F_{max}$ is the maximum load in MPa and b, h and L are the width, height and span length of the tested specimens, being equal to 50 mm, 50 mm and 150 mm respectively. The highest peak strength was found for the mortar control mixture (e.g. 6.1 MPa). The addition of 10 vol% and 20 vol% of PCMs reduced the peak strength to 4.0 MPa and 3.0 MPa, respectively, as shown in Figure 9a. The cenosphere control mixture exhibited a strength of 3.3 MPa with a reduction to 2.5 MPa for 10 vol% and a reduction to 2.3 MPa for 20 vol% of incorporated PCMs. The lattice samples showed a strength of 3.1 MPa and 2.5 MPa for the mortar and cenosphere mixture, respectively. Figure 9b reveals the change in strength compared to the mortar and cenosphere control samples.

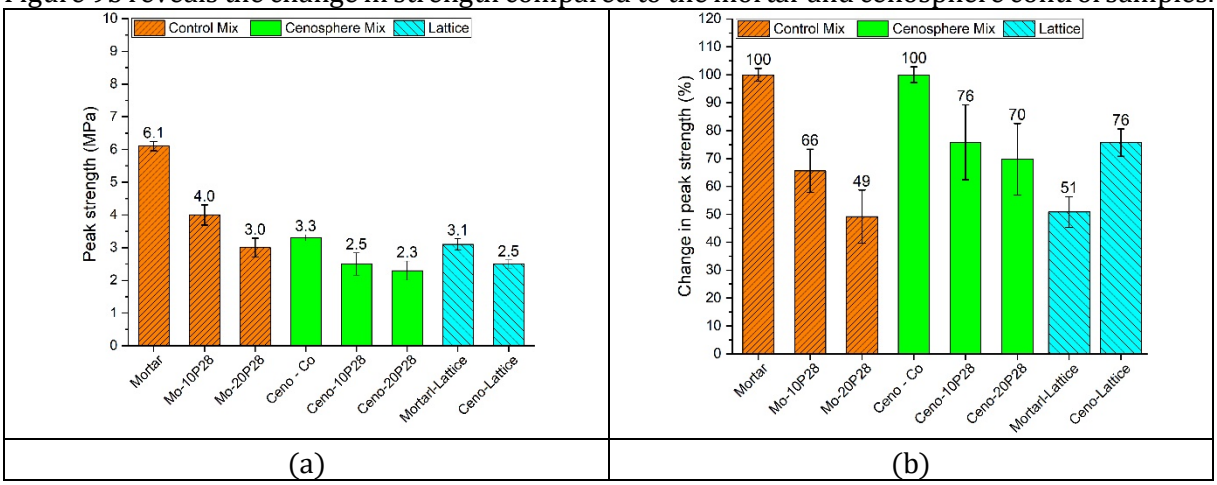


Figure 9: Flexural peak strength a) for all samples in MPa, b) change in peak strength compared to the mortar and cenosphere control samples in %.

### 3.2 Differential Scanning Calorimetry (DSC)

Table 5 lists the results of the DSC for the pure and encapsulated paraffin. The pure paraffin is the paraffin that was incorporated into the hollow 3D-printed lattices. The sample mass of each test is given in Table 5. The heat storage capacity given in Table 5 is the result of the integral of the heat capacity in J/(g °C) shown in Figure 10. The encapsulated PCM shows a higher heat storage capacity compared to the pure paraffin. It would be expected that the pure paraffin shows a higher heat storage capacity than the micro-encapsulated PCM. However, the exact composition of both PCM products (Nextek 28D and PCM28) was not reviled by the supplier (Microtek Laboratories in Dayton, USA) and therefore it is assumed that the paraffin used for the encapsulated product differs from the pure product and therefore a lower heat capacity is measured for the pure paraffin.

Table 5: DSC results obtained within a temperature range of 10 to 60 °C

| Sample | Sample mass | Heat storage capacity[1] | Peak Temperature | Heat Capacity at peak temperature |
|---|---|---|---|---|
| | mg | J / g | °C | J/g°C |
| PureParaffin28 | 67.5 | 206.4 | 26.65 | 49.62 |
| Encapsulated Paraffin | 66.2 | 216.2 | 26.75 | 57.55 |

[1]Combination of latent heat and sensible heat measured in a temperature range of 15 to 40 °C

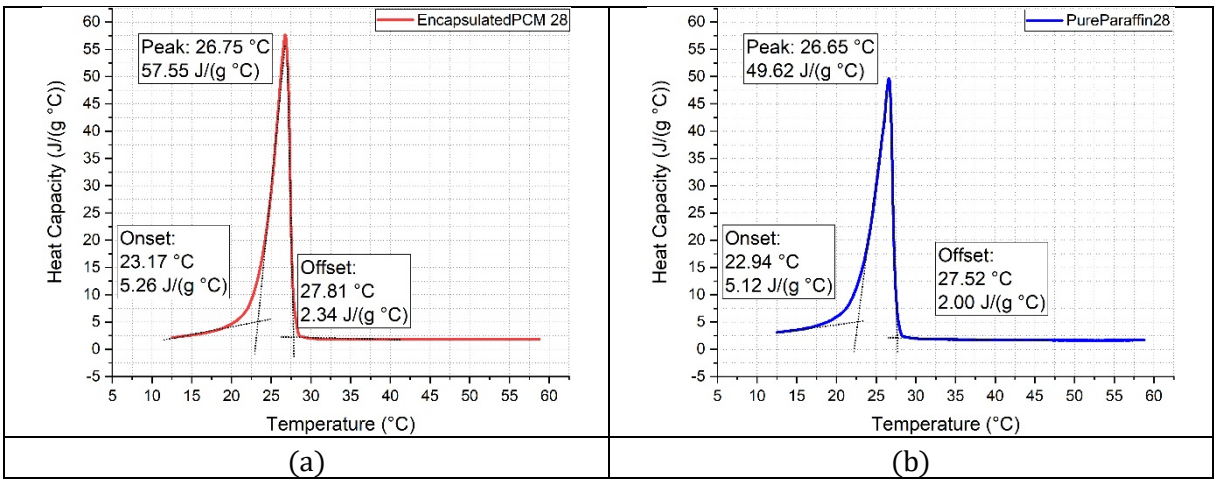


Figure 10: Heat capacity of tested specimens in J/(g °C), a) Encapsulated PCM for concrete mixtures, b) pure paraffin for hollow lattice

## 3.3 Thermal performance of panels – Hot Box Test

### 3.3.1 Heat flux measurement

The heat flux into the mortar and cenosphere samples during the 90-minute heating period is shown in Figure 11. While both samples reached the desired heat flux of 500W/m² after 10 minutes, the cenosphere samples exhibited a faster drop in heat flux during the remaining heating period. A detailed discussion of the thermal behavior and correlation of heat flux and temperature developments are given in the following section.

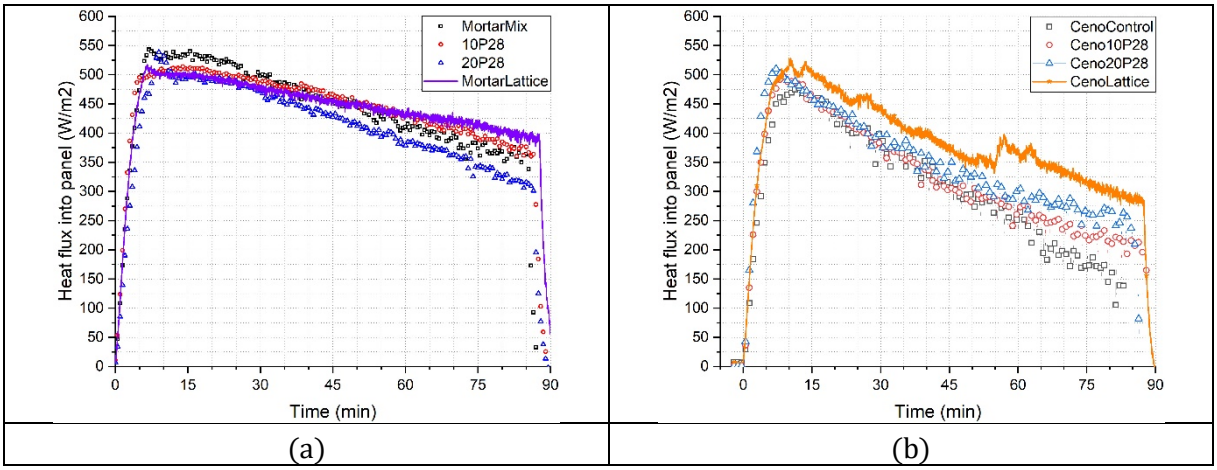


Figure 11: Heat flux from the radiant heater into the panels over the heating period of 90 min in W/m² a) heat flux into the Mortar panels, b) heat flux into the cenosphere panels

The heat flux of the mortar and cenosphere samples into the test chamber over the test period of 180 min are shown in Figure 12. The control samples show a steady increase over the heating period which is followed by a decrease thereafter. Mixtures with incorporated PCMs show a reduced heat flux path as well as the time shift of its peak. Furthermore, mixtures with PCMs show a slower increase within the first 70 minutes of the heating period which turns into a steeper increase thereafter. Mixtures containing 10% PCMs show this steep increase earlier than mixtures with 20% PCM or the lattice mixtures. This can be attributed to the charging phase of the PCMs. The heat flux increases slowly during the time where the PCMs melt but as soon as the PCMs are fully melted and cannot store any more energy the heat flux starts to sharply increase. It should

be noted that the cenosphere samples exhibit a small variation in the heat flux peak. This stems from the variation of the heat flux into the panels over the heating period, as shown in Figure 11, where the control panel exhibited the lowest heat flux during the heating period and the lattice sample the highest. More details about the cumulative heat flux and the performance of the lattice samples will be given in Section 4.

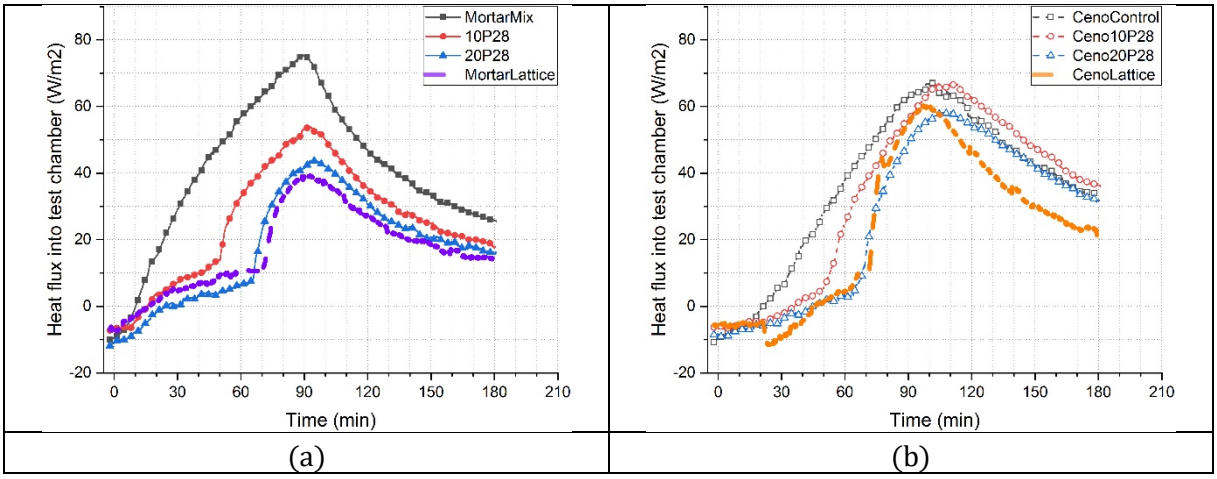


(a) (b)

Figure 12: Heat flux from the panel into the test chamber a) Mortar mixtures; b) Cenosphere mixtures

### 3.3.2 Temperature development

#### 3.3.2.1 Temperature within the reflective tunnel

The ambient temperature was recorded within the reflective tunnel at a distance of 2 cm from the heated surface of the specimens and are presented in Figure 13. The cenosphere mixtures exhibit overall higher ambient temperatures than the mortar mixtures. The higher ambient temperatures for the cenosphere mixtures compared to the mortar mixtures are also in compliance with the measured higher surface temperature as shown in Figure 14 which results in a higher emitted radiation of the cenosphere panels back to the temperature sensor. This emitted radiation contributes to the urban heat island effect which increases the daytime temperature of the surrounding area and therefore reduced the nighttime cooling of a metropolitan area. This becomes a concerning matter in cities with a high number of reflecting surfaces. The presented results show that a higher amount of PCMs result in a lower ambient temperature whereas the specimens with the incorporated lattices show the lowest ambient temperatures. A further reduction of the high radiation and surface temperature could be provided with a cool color coating of the panels as investigated in [49] and could further reduce the urban heat island effect.

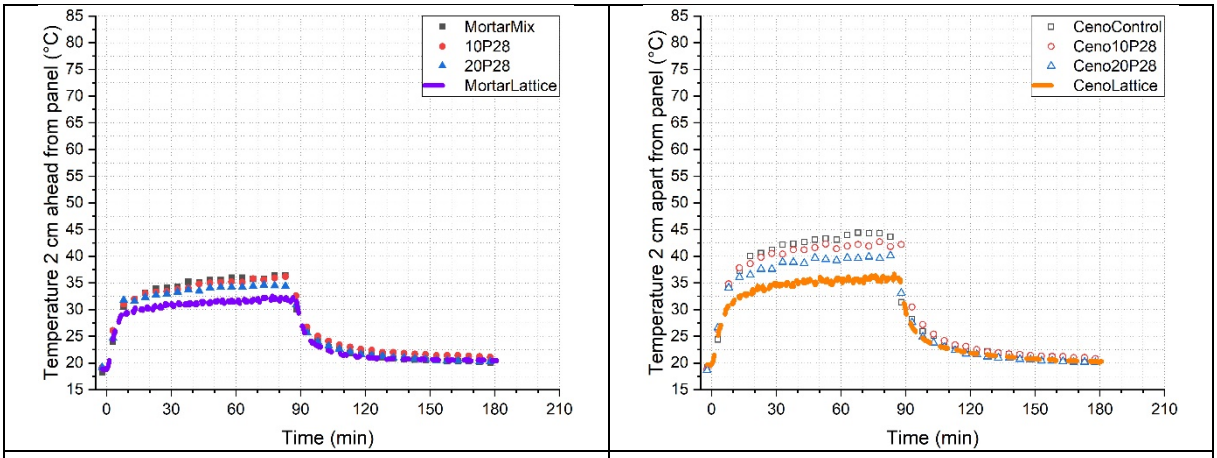


(a) (b)

Figure 13: Temperature history on the heated side, measured at a distance of 2 cm in front of the heated surface of the panel a) temperature development for the mortar samples, b) temperature development for the cenosphere samples

### 3.3.2.2 Surface temperatures

The surface temperature of the mortar and cenosphere panels facing the heating panel (exterior surface of the panels) are shown in Figure 14a and Figure 15a, respectively. The surface temperature of the mortar and cenosphere panels facing the test chamber (interior surface of the panels) are shown in Figure 14b and Figure 15b, respectively.

The mortar control mixture shows a surface temperature of 57.9 °C after a heating period of 90 min and an interior surface temperature of 47.6 °C, hence exhibiting a temperature gradient of 10.3 °C within the 5 cm thick sample (see Figure 14). The PCMs reduce the interior surface temperatures with increasing amount. 10 vol% of PCMs result into 40.8 °C, 20 vol% into 37.4 °C for the interior surfaces. The lowest interior surface temperature is recorded for the lattice specimen with 33.8 °C (see Figure 14b). The exterior surface temperature does not show the same behavior for the micro-encapsulated panels. Addition of 10 and 20 vol % shows similar surface temperatures of 52.9 °C and 53.5 °C respectively but the lattice sample shows a significant lower surface temperature of 45.3 °C (see Figure 14a). This effect will be discussed later on in section 4.

The cenosphere mixtures show a similar behavior where the internal surface temperature decreased with increasing amount of PCMs. 10 vol % result into an interior surface temperature of 51.4 °C, 20 vol % into 42.2 °C (see Figure 15b). The lowest interior surface temperature was recorded for the lattice sample showing 36.8 °C. The exterior surface temperature however shows somewhat controversial results with the highest temperature for the 10 vol% of PCM (81.1 °C) followed by the control mixture (76.1 °C) and the 20 vol % PCM mixture (75.0 °C). This could be an effect of the varying cumulative heat flux applied to the panels where the control mix exhibited the lowest cumulative heat flux. Further details will be discussed in section 4.

The heat storage effect of the PCMs can be seen on the internal surface temperature (Figure 12). The control mixes show a steady increase during the heating period whereas the mixtures containing PCMs show a slower increase of the internal surface temperature due to the heat absorption of the PCMs. At the point where the PCMs are melted the surface temperature increases significantly faster. This inflection point appears first for the 10 vol % PCM mixture followed by the 20 vol % and the lattice sample (see Figure 14b and Figure 15b). Additionally, the heat storage effect results in a shift of the peak surface temperature at the internal surface. The mortar mixtures with 10 and 20 vol % show a shift of 4.8 and 9.2 minutes respectively. The mortar

lattice mixture shows as peak shift of 12.0 minutes compared to the control mixture. A shift of 7.8 and 9.5 minutes for 10 and 20 vol % was observed for the cenosphere mixtures. Due to the steep increase of surface temperature of the cenosphere lattice panel a shift in the peak temperature of only 1.0 minutes could be recorded (see and Figure 15b).

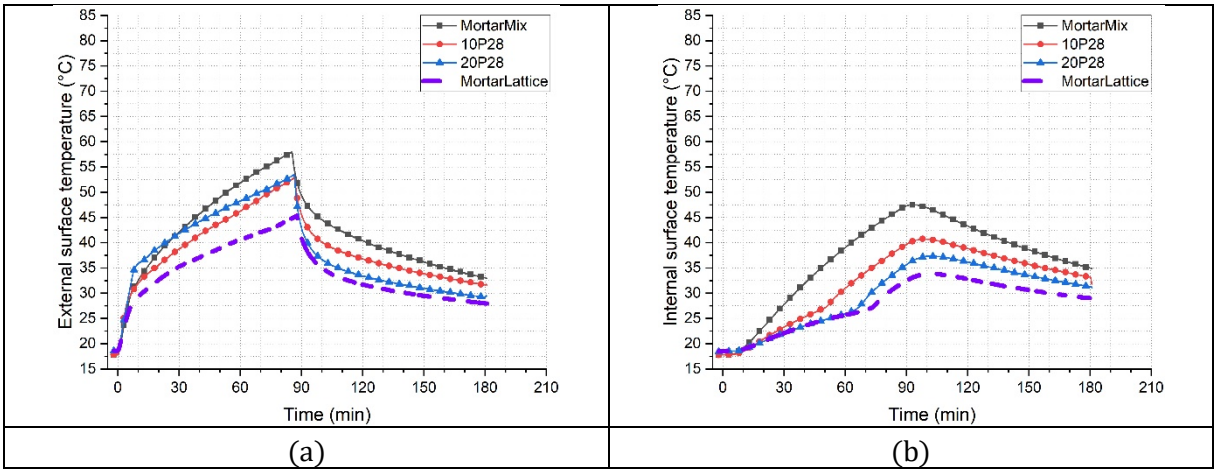


Figure 14: Surface temperature of the panels a) external (heated) side, b) internal side (inside test chamber)

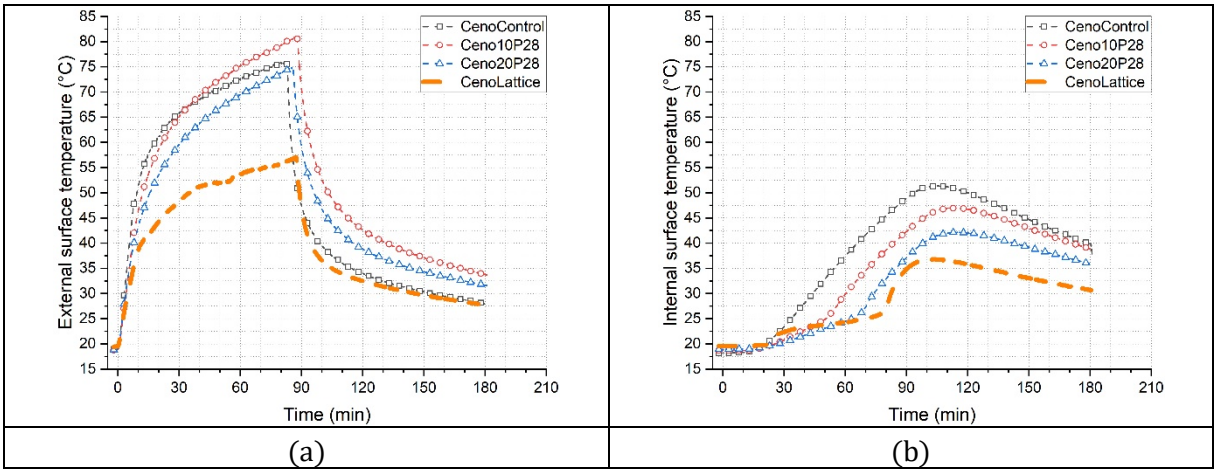


Figure 15: Surface temperature of the panels a) external (heated) side, b) internal side (inside test chamber)

### 3.3.2.3 Test Chamber Temperature

Results of the mortar and cenosphere chamber temperature are shown in Figure 16 where a reduction of the chamber temperature with increasing PCM amount can be seen. Mortar mixtures without PCMs exhibit a temperature of 47.6 °C whereas the inclusion of 10 vol% and 20 vol% PCMs reduced the temperature to 40.8 °C and 37.4 °C, respectively. A significant lower peak temperature of 30.6 °C during the test period was recorded for the mortar lattice specimen and proves the beneficial effect of this macro-encapsulation method. Similar characteristics are observed for the cenosphere mixtures with a peak chamber temperature of 47.0 °C and 42.2 °C for 10 vol% and 20 vol% of PCMs and 31.2 °C for the lattice specimen compared to the cenosphere control mixture with a maximum chamber temperature of 51.4 °C.

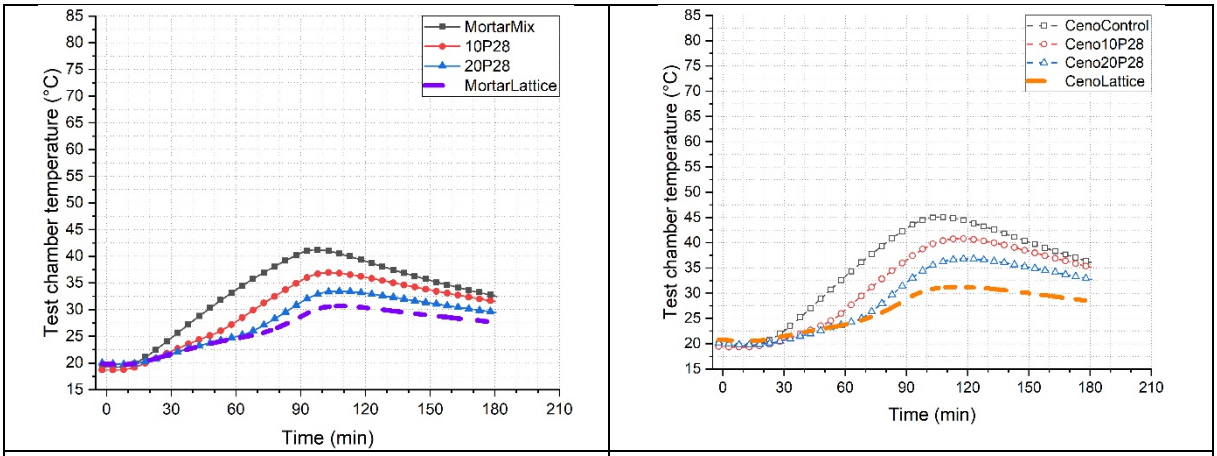


411 Figure 16: Test chamber temperature a) mortar mixtures b) cenosphere mixtures
412

413 # 4 Discussion

414 ## 4.1 Surface temperature

415 The external surface temperature measurements revealed a significant higher temperature for
416 the cenosphere control panels (max. temp. of 81.1 °C) than for the mortar control panels (max.
417 temp. of 57.9°C) as shown in Figure 17a, even though the initial conditions for all samples were
418 kept at 500 W/m² for the first 10 minutes of the heating period. To compare the heat fluxes into
419 the panel the cumulative heat flux over the heating period is calculated and shown in Figure 17b.
420 The cumulative heat flux represents the integral of the heat flux (W/m²) (Figure 12) and is
421 presented in (W/m²) hr. The results show very similar heat fluxes during the first 20 minutes of
422 the heating period but varies for the different mixtures thereafter. These varying cumulative heat
423 fluxes contribute to the different evolution of the surface temperature and to some extent can be
424 related to the discussed external surface temperatures within a mixture. E.g. the cenosphere panel
425 with 10 vol % PCMs shows a higher surface temperature than the control panel after 90 minutes
426 of heating since the panel with 10 vol % of PCMs exhibits a higher cumulative heat flux at this time
427 instant (see Figure 17a and b). Further parameters influencing the differences in surface
428 temperature and heat fluxes are discussed below.
429

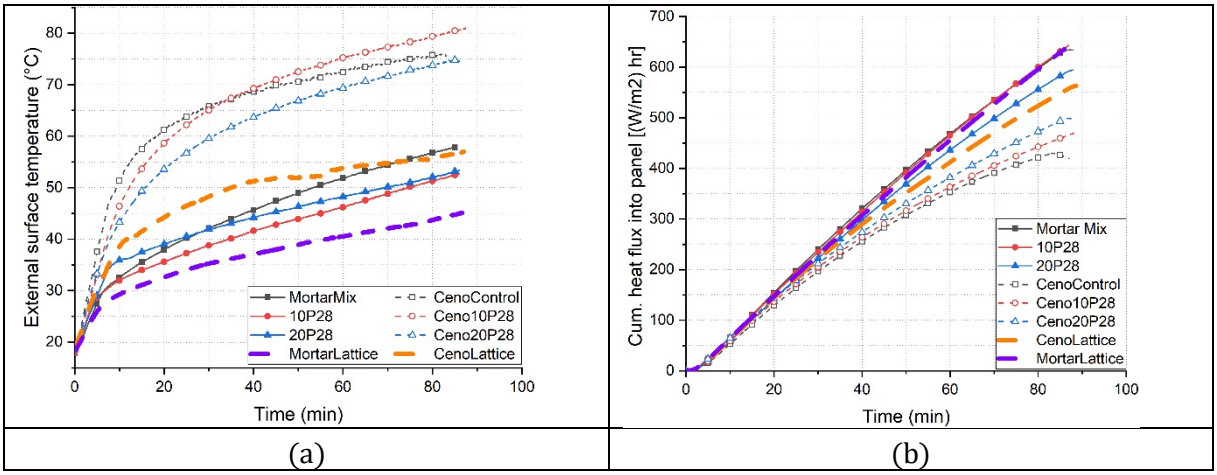


430 Figure 17: a) Development of external surface temperature and b) cumulative heat flux from the
431 radiant heater into the panels within the heating period of 90 minutes
432
433

A reason for the difference in the maximum surface temperatures between the cenosphere panels and the mortar panels (which contain sand as fine aggregates) is the difference in thermal conductivity of the constituents. Table 6 lists the thermal conductivity of the mix constituents and reveals the significant difference in thermal conductivity for sand (4.0 W/mK) and cenospheres (0.18 W/mK). A lower thermal conductivity of the cenosphere panels is caused by the lack of sand in these mixtures.

Table 6: Thermal conductivity of constituents and sources

| Constituent | Thermal conductivity [W/mK] | Source |
|---|---|---|
| Water | 0.60 | Ramires et al. [54] |
| Cement | 1.55 | Bentz [55] |
| Sand | 4.00 | Robertson [56] |
| Cenosphere | 0.18 | Datasheet [57] |
| PCM | 0.21-0.23 | Cui et al.[19] |
| ABS | 0.17 | Compton et al. [58] |
| Lightweight concrete density 1280 kg/m3 | 0.48-0.59 | Tara et al. [59] |
| Concrete Density 2080-2250 kg/m3 | 1.0-2.0 | Tara et al. [59] Shafigh [60]et al. |

Due to the temperature difference between the external and internal surface during heating a non-steady state is achieved within the panels and transient conduction takes place. The heat conduction is described by Fourier's law which describes the heat transfer through a material as:

$$q = -k\,\nabla T \tag{2}$$

where q is the heat flux in ($W/m^2$), k the thermal conductivity in (W/m K) and ∇T the temperature gradient in Kelvin/meter. For a constant temperature difference (e.g. constant external to internal temperature) the heat flux into a material depends on its thermal conductivity (see equation 2). The higher the thermal conductivity, the higher the heat flux into the specimen. This behavior is observed for the investigated panels and shown by the cumulative heat flux in Figure 17b where all mortar panels (with and without PCMs) exhibit a higher heat flux over the 90 min heating period compared to the cenosphere panels. Furthermore, a material with a higher thermal conductivity is able to transport the heat at the surface faster into the material which results in a lower surface temperature. This effect was observed for all mortar panels which exhibited lower surface temperatures compared to the cenosphere panels and is in compliance with experimental results found by Ng et. al. in [61]. Quin [62] numerically investigated the surface temperature of concrete pavements and their correlation to the thermal conductivity. Quin's results also revealed lower surface temperatures with increasing thermal conductivity. The lowest surface temperatures were observed for the lattice panels which would, based on the discussions above, indicate that their thermal conductivities are higher than those of the control mixes. However, replacing 22 % of the cementitious matrices by the ABS lattice (which has a much lower k as shown in Table 6) should decrease, not increase the thermal conductivity. Hence, besides the thermal conductivity, other parameters must influence the external temperature of the panels.

### 4.1.1 Effect of volumetric heat capacity

Besides the thermal conductivity, the volumetric heat capacity, $C_V$, in $kJ/(m^3\,K)$ was found by [62, 63] to additionally influence the surface temperature of a material where a higher $C_v$ results in a lower surface temperature. The volumetric heat capacity is defined as

$$C_V = \rho \cdot c_p \quad (3)$$

where $\rho$ is the density in kg/m$^3$ and $C_p$ the specific heat in J/(kg K). A difference in density was indeed observed between each mixture due to the replacement of aggregates by cenospheres and PCMs (see Table 8). The mortar panels exhibit a reduction in density whereas the cenosphere panels exhibit a slight increase in density with increasing replacement of cenospheres by PCMs due to the slightly higher densities of PCMs compared to cenospheres. According to a literature review done by Shafigh et al. [60] the specific heat capacity of mortar and lightweight concrete is in the range of 0.932-0.951 and 0.840-0.951 respectively. Taking the mean values of $C_p$ and considering the measured density of the mortar and cenosphere control mixtures the volumetric heat capacity of the matrix can be calculated according to equation 3 and shows a higher $C_v$ for the mortar matrix compared to the cenosphere matrix as shown in Table 7. This results also strengthen the hypothesis that the combination of the higher thermal conductivity and the higher volumetric heat capacity results in a lower surface temperature for the mortar panels. It should be noted that for this comparison only the control mixtures were assessed since those do not contain PCMs which would increase the heat capacity of the sample.

Table 7: Specific and volumetric heat capacity of mortar and cenosphere control samples

| Specimen | Density | Cp[1] | Cv |
|---|---|---|---|
| | Kg/m$^3$ | kJ/kg K | kJ/m$^3$ K |
| Mortar matrix | 2161 | 0.941 | 2.03 |
| Cenosphere matrix | 1351 | 0.895 | 1.21 |

[1]Mean values taken from reference [60]

Due to the minor differences observed in the surface temperatures within the mortar and cenosphere panels with and without micro-encapsulated PCMs one may conclude that the micro-encapsulated PCMs have little effect on the surface temperature of the panels. This may to some extent be due to a lower volume fraction of PCMs on the surface (i.e. due to the wall effect which forms a thin layer of cement paste due to the vibration process). Therefore, micro-encapsulated PCMs may not significantly enhance the heat capacity of the surface layers (see Table 8) but further investigation of the influence of micro-encapsulated PCMs on the surface temperature is needed but was not within the scope this project.

Table 8: Density and surface temperature of the mortar and cenosphere samples with and without PCMs

| Specimen | Mass [kg] | Density [kg/m$^3$] | Peak surface external[1] [°C] |
|---|---|---|---|
| MortarMix | 9.7 | 2161 | 57.9 |
| 10P28 | 9.2 | 2044 | 52.9 |
| 20P28 | 8.6 | 1916 | 53.5 |
| **MortarLattice** | **8.0** | **1778** | **45.3** |
| CenoControl | 6.1 | 1351 | 76.1 |
| Ceno10P28 | 6.2 | 1372 | 81.1 |
| Ceno20P28 | 6.2 | 1373 | 75.0 |
| **Ceno Lattice** | **5.4** | **1197** | **57.1** |

[1]Surface exposed to heating

It should be noted that the numerical investigations performed by [62, 63] showed that the change in reflectivity of the material has a higher influence on the surface temperature than a change in the volumetric heat capacity. However, in this study the investigated panels have very similar color, therefore, a difference in surface temperature is not expected due to this effect.

## 4.2 Temperature development

The temperature difference of the specimens external and internal surface is shown in Figure 18. The cenosphere mixtures exhibit higher temperature differences which can be explained by the lower thermal conductivity and volumetric heat capacity of the lightweight concrete compared to the mortar panels as discussed earlier. All panels in Figure 18 show a linear increase of the temperature difference at the beginning of the heating period which is followed by a decrease of the gradient till a maximum is reached. Thereafter a decrease in the temperature difference between external and internal surface is recorded. The time at which the temperature difference starts to decrease occurs at the earliest for the control mixtures, at 25 minutes for the mortar and at 30 minutes for the cenosphere mixture. For the samples containing 10 vol % of PCM the point in time where the decrease of the temperature difference starts is at 52-53 minutes for both, the mortar and the cenosphere panels. A matching point in time for the decrease was also found for the 20 vol % PCM panels at 67-69 minutes. The lattice samples show their start of the linear decrease very close to the end of the heating period at 75 and 80 minutes for the mortar and cenosphere mix, respectively (see Figure 18). At this time instants the heat starts to pass faster through the panels and is related to the amount of PCMs. The higher the amount of PCM the more heat can be absorbed which results in a time delay where the heat passes faster through the panels. As a result, the interior room temperature will increase slower.

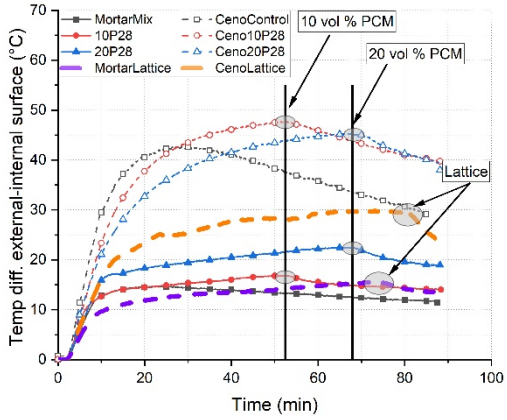


Figure 18: Temperature difference between external and internal surfaces of the panels

The panel's performance can be assessed by comparing the temperature increase of the panels, $T_{inc}$, to the applied energy on the exterior surface (see Figure 19). The temperature increase of the panels is calculated by

$$T_{inc} = \Delta T - T_{initial} \quad (4)$$

where $\Delta T$ is the temperature difference of the external to internal surface and $T_{initial}$ the temperature of the unheated specimen at the beginning of the test. This presentation allows the evaluation of the panel's temperature increase for each given input energy and shows the lowest temperature increase for the lattice panels at any input energy.

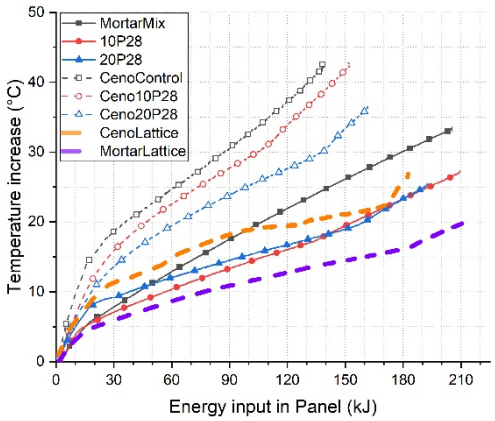


Figure 19: Temperature increase of the panels due to the applied energy to the external surface

### 4.3 Chamber temperature and time lag

Figure 20 compares the peak temperature and their peak time difference of the lattice samples to the control panels of the mortar and cenosphere mixture. A temperature decreases of 10.6°C and 13.9°C and a time lag of 10 min and 9 min for the 50 mm thick panels is recorded for the mortar and cenosphere mixture respectively and shows the beneficial effect of the lattice sample filled with pure paraffin.

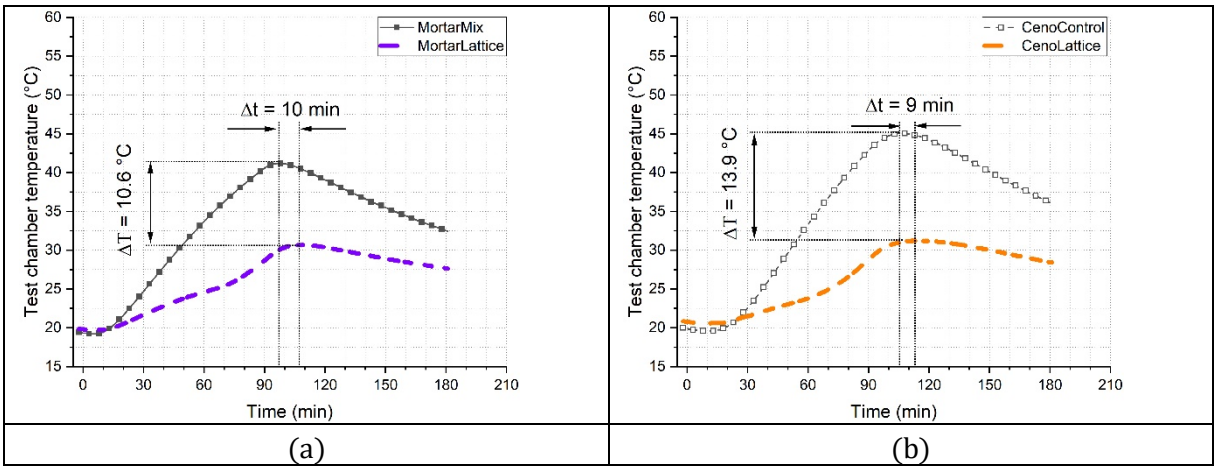


Figure 20: Comparison of the time lag and peak temperature difference of the lattice and control panels measured within the test chamber for a) the mortar panels and b) the cenosphere panels

## 5 Conclusion

A 3D printed hollow lattice was developed to serve as macro-encapsulation for Phase-Change-Materials (PCMs). Panels containing the lattices were prepared with either a mortar mixture or a lightweight mixture containing cenospheres as aggregates. To evaluate the benefit of the PCM-lattice, control specimens without PCM and with micro-encapsulated PCMs were fabricated and tested. The thermal properties were investigated by means of Differential Scanning Calorimetry (DSC) analysis and Hot Box tests. The mechanical properties were evaluated by performing compression and bending test.

The indoor temperature of the test chamber could be reduced by 13.9 °C and 10.6 °C with a 50 mm thick PCM filled lattice panel compared to the control panels. This reveals the potential of this system to be used for thermal retrofitting of existing houses. Furthermore, the PCM filled lattice panels showed the highest energy absorption and develop the lowest panel temperatures during

heating. Therefore, the lattice system can reduce the urban heat island effect which contributes to an increase of the surrounding air temperature of a metropolitan area. The PCM-lattice samples significantly improved the post cracking behavior of the specimens. The PCM-lattice specimens show a ductile and strain-hardening behavior instead of a brittle failure mode which was observed for the control mixtures. This study reveals the benefits of a PCM-filled lattice incorporated into cement-based matrices on the thermal and flexural performance which can be used either for retrofitting or as new exterior wall systems to reduce the indoor temperature and electricity consumption for space cooling. Furthermore, the developed 3D printed lattice structure allows an optimization of the location and amount of the used PCMs. The mechanical and thermal performance of the lattice can be improved by using different materials and optimizing the lattice geometry and is subject of ongoing research.

## Acknowledgements

This research is funded by the Republic of Singapore's National Research Foundation through a grant to the Berkeley Education Alliance for Research in Singapore (BEARS) for the Singapore-Berkeley Building Efficiency and Sustainability in the Tropics (SinBerBEST) Program. BEARS has been established by the University of California, Berkeley, as a center for intellectual excellence in research and education in Singapore.

## 6 References

[1] G. Happle, E. Wilhelm, J. A. Fonseca, and A. Schlueter, "Determining air-conditioning usage patterns in Singapore from distributed, portable sensors," *Energy Procedia,* vol. 122, pp. 313-318, 2017/09/01/ 2017, doi: https://doi.org/10.1016/j.egypro.2017.07.328.

[2] N. H. Wong and S. S. Khoo, "Thermal comfort in classrooms in the tropics," *Energy and Buildings,* vol. 35, no. 4, pp. 337-351, 2003/05/01/ 2003, doi: https://doi.org/10.1016/S0378-7788(02)00109-3.

[3] R. Baetens, B. P. Jelle, and A. Gustavsen, "Phase change materials for building applications: A state-of-the-art review," *Energy and Buildings,* vol. 42, no. 9, pp. 1361-1368, 2010/09/01/ 2010, doi: https://doi.org/10.1016/j.enbuild.2010.03.026.

[4] F. Kuznik, D. David, K. Johannes, and J.-J. Roux, "A review on phase change materials integrated in building walls," *Renewable and Sustainable Energy Reviews,* vol. 15, no. 1, pp. 379-391, 2011/01/01/ 2011, doi: https://doi.org/10.1016/j.rser.2010.08.019.

[5] V. V. Tyagi, S. C. Kaushik, S. K. Tyagi, and T. Akiyama, "Development of phase change materials based microencapsulated technology for buildings: A review," *Renewable and Sustainable Energy Reviews,* vol. 15, no. 2, pp. 1373-1391, 2011/02/01/ 2011, doi: https://doi.org/10.1016/j.rser.2010.10.006.

[6] W. Xiao, X. Wang, and Y. Zhang, "Analytical optimization of interior PCM for energy storage in a lightweight passive solar room," *Applied Energy,* vol. 86, no. 10, pp. 2013-2018, 2009/10/01/ 2009, doi: https://doi.org/10.1016/j.apenergy.2008.12.011.

[7] D. Zhou, C. Y. Zhao, and Y. Tian, "Review on thermal energy storage with phase change materials (PCMs) in building applications," *Applied Energy,* vol. 92, pp. 593-605, 2012/04/01/ 2012, doi: https://doi.org/10.1016/j.apenergy.2011.08.025.

[8] S.-G. Jeong, S. Wi, S. J. Chang, J. Lee, and S. Kim, "An experimental study on applying organic PCMs to gypsum-cement board for improving thermal performance of buildings in different climates," *Energy and Buildings,* vol. 190, pp. 183-194, 2019/05/01/ 2019, doi: https://doi.org/10.1016/j.enbuild.2019.02.037.

[9] U. Berardi and S. Soudian, "Experimental investigation of latent heat thermal energy storage using PCMs with different melting temperatures for building retrofit," *Energy and Buildings,* vol. 185, pp. 180-195, 2019/02/15/ 2019, doi: https://doi.org/10.1016/j.enbuild.2018.12.016.

[10] P. A. Fokaides, A. Kylili, and S. A. Kalogirou, "Phase change materials (PCMs) integrated into transparent building elements: a review," *Materials for Renewable and Sustainable Energy,* vol. 4, no. 2, p. 6, 2015/04/02 2015, doi: 10.1007/s40243-015-0047-8.

[11] K. O. Lee, M. A. Medina, X. Sun, and X. Jin, "Thermal performance of phase change materials (PCM)-enhanced cellulose insulation in passive solar residential building walls," *Solar Energy,* vol. 163, pp. 113-121, 2018/03/15/ 2018, doi: https://doi.org/10.1016/j.solener.2018.01.086.

[12] J. H. Park, J. Jeon, J. Lee, S. Wi, B. Y. Yun, and S. Kim, "Comparative analysis of the PCM application according to the building type as retrofit system," *Building and Environment,* vol. 151, pp. 291-302, 2019/03/15/ 2019, doi: https://doi.org/10.1016/j.buildenv.2019.01.048.

[13] J. Guo, J. Dong, B. Zou, H. Wang, L. Zhu, and Y. Jiang, "Experimental investigation on the effects of phase change material and different ventilation modes on the thermal storage, space heating and energy consumption characteristics of ventilated mortar blocks," *Journal of Energy Storage,* vol. 41, p. 102817, 2021/09/01/ 2021, doi: https://doi.org/10.1016/j.est.2021.102817.

[14] A. M. Heniegal, O. M. Omar Ibrahim, N. B. Frahat, and M. Amin, "New techniques for the energy saving of sustainable buildings by using phase change materials," *Journal of Building Engineering,* vol. 41, p. 102418, 2021/09/01/ 2021, doi: https://doi.org/10.1016/j.jobe.2021.102418.

[15] R. Cai, Z. Sun, H. Yu, E. Meng, J. Wang, and M. Dai, "Review on optimization of phase change parameters in phase change material building envelopes," *Journal of Building Engineering,* vol. 35, p. 101979, 2021/03/01/ 2021, doi: https://doi.org/10.1016/j.jobe.2020.101979.

[16] H. Akeiber *et al.*, "A review on phase change material (PCM) for sustainable passive cooling in building envelopes," *Renewable and Sustainable Energy Reviews,* vol. 60, pp. 1470-1497, 2016/07/01/ 2016, doi: https://doi.org/10.1016/j.rser.2016.03.036.

[17] C. Alkan, "Enthalpy of melting and solidification of sulfonated paraffins as phase change materials for thermal energy storage," *Thermochimica Acta,* vol. 451, no. 1, pp. 126-130, 2006/12/01/ 2006, doi: https://doi.org/10.1016/j.tca.2006.09.010.

[18] A. Sharma, S. D. Sharma, and D. Buddhi, "Accelerated thermal cycle test of acetamide, stearic acid and paraffin wax for solar thermal latent heat storage applications," *Energy Conversion and Management,* vol. 43, no. 14, pp. 1923-1930, 2002/09/01/ 2002, doi: https://doi.org/10.1016/S0196-8904(01)00131-5.

[19] H. Cui, W. Liao, X. Mi, T. Y. Lo, and D. Chen, "Study on functional and mechanical properties of cement mortar with graphite-modified microencapsulated phase-change materials," *Energy and Buildings,* vol. 105, pp. 273-284, 2015/10/15/ 2015, doi: https://doi.org/10.1016/j.enbuild.2015.07.043.

[20] A. Sarı and A. Karaipekli, "Thermal conductivity and latent heat thermal energy storage characteristics of paraffin/expanded graphite composite as phase change material," *Applied Thermal Engineering,* vol. 27, no. 8, pp. 1271-1277, 2007/06/01/ 2007, doi: https://doi.org/10.1016/j.applthermaleng.2006.11.004.

[21] F. Frusteri, V. Leonardi, S. Vasta, and G. Restuccia, "Thermal conductivity measurement of a PCM based storage system containing carbon fibers," *Applied Thermal Engineering,* vol. 25, no. 11, pp. 1623-1633, 2005/08/01/ 2005, doi: https://doi.org/10.1016/j.applthermaleng.2004.10.007.

[22] A. Mills, M. Farid, J. R. Selman, and S. Al-Hallaj, "Thermal conductivity enhancement of phase change materials using a graphite matrix," *Applied Thermal Engineering,* vol. 26, no. 14, pp. 1652-1661, 2006/10/01/ 2006, doi: https://doi.org/10.1016/j.applthermaleng.2005.11.022.

[23] W. Wang, X. Yang, Y. Fang, J. Ding, and J. Yan, "Preparation and thermal properties of polyethylene glycol/expanded graphite blends for energy storage," *Applied Energy,* vol. 86, no. 9, pp. 1479-1483, 2009/09/01/ 2009, doi: https://doi.org/10.1016/j.apenergy.2008.12.004.

[24] Z. Zhang and X. Fang, "Study on paraffin/expanded graphite composite phase change thermal energy storage material," *Energy Conversion and Management,* vol. 47, no. 3, pp. 303-310, 2006/02/01/ 2006, doi: https://doi.org/10.1016/j.enconman.2005.03.004.

[25] M. Li, Z. Wu, H. Kao, and J. Tan, "Experimental investigation of preparation and thermal performances of paraffin/bentonite composite phase change material," *Energy Conversion and Management,* vol. 52, no. 11, pp. 3275-3281, 2011/10/01/ 2011, doi: https://doi.org/10.1016/j.enconman.2011.05.015.

[26] L. Liu *et al.*, "Experimental study on preparation of a novel foamed cement with paraffin/ expanded graphite composite phase change thermal energy storage material," *Energy Procedia,* vol. 158, pp. 4799-4804, 2019/02/01/ 2019, doi: https://doi.org/10.1016/j.egypro.2019.01.717.

[27] X. Zhou, H. Xiao, J. Feng, C. Zhang, and Y. Jiang, "Preparation and thermal properties of paraffin/porous silica ceramic composite," *Composites Science and Technology,* vol. 69, no. 7, pp. 1246-1249, 2009/06/01/ 2009, doi: https://doi.org/10.1016/j.compscitech.2009.02.030.

[28] F. Liu, J. Wang, and X. Qian, "Integrating phase change materials into concrete through microencapsulation using cenospheres," *Cement and Concrete Composites,* vol. 80, pp. 317-325, 2017/07/01/ 2017, doi: https://doi.org/10.1016/j.cemconcomp.2017.04.001.

[29] P. Sukontasukkul *et al.*, "Thermal properties of lightweight concrete incorporating high contents of phase change materials," *Construction and Building Materials,* vol. 207, pp. 431-439, 2019/05/20/ 2019, doi: https://doi.org/10.1016/j.conbuildmat.2019.02.152.

[30] G. F. Huseien and A. R. M. Sam, "Nanostructures encapsulated phase change materials for sustained thermal energy storage in concrete: An overall assessment," *Materials Today: Proceedings,* vol. 42, pp. 2457-2463, 2021/01/01/ 2021, doi: https://doi.org/10.1016/j.matpr.2020.12.563.

[31] H. Ettouney, I. Alatiqi, M. Al-Sahali, and K. Al-Hajirie, "Heat transfer enhancement in energy storage in spherical capsules filled with paraffin wax and metal beads," *Energy Conversion and Management,* vol. 47, no. 2, pp. 211-228, 2006/01/01/ 2006, doi: https://doi.org/10.1016/j.enconman.2005.04.003.

[32] L. F. Cabeza, A. Castell, C. Barreneche, A. de Gracia, and A. I. Fernández, "Materials used as PCM in thermal energy storage in buildings: A review," *Renewable and Sustainable Energy Reviews,* vol. 15, no. 3, pp. 1675-1695, 2011/04/01/ 2011, doi: https://doi.org/10.1016/j.rser.2010.11.018.

[33] F. L. Tan, S. F. Hosseinizadeh, J. M. Khodadadi, and L. Fan, "Experimental and computational study of constrained melting of phase change materials (PCM) inside a spherical capsule," *International Journal of Heat and Mass Transfer,* vol. 52, no. 15, pp. 3464-3472, 2009/07/01/ 2009, doi: https://doi.org/10.1016/j.ijheatmasstransfer.2009.02.043.

[34] A. Marani and M. Madhkhan, "Thermal performance of concrete sandwich panels incorporating phase change materials: An experimental study," *Journal of Materials Research and Technology,* vol. 12, pp. 760-775, 2021/05/01/ 2021, doi: https://doi.org/10.1016/j.jmrt.2021.03.022.

[35] Q. Al-Yasiri and M. Szabó, "Thermal performance of concrete bricks based phase change material encapsulated by various aluminium containers: An experimental study under Iraqi hot climate conditions," *Journal of Energy Storage,* vol. 40, p. 102710, 2021/08/01/ 2021, doi: https://doi.org/10.1016/j.est.2021.102710.

[36] C.-m. Lai, R. H. Chen, and C.-Y. Lin, "Heat transfer and thermal storage behaviour of gypsum boards incorporating micro-encapsulated PCM," *Energy and Buildings,* vol. 42, no. 8, pp. 1259-1266, 2010/08/01/ 2010, doi: https://doi.org/10.1016/j.enbuild.2010.02.018.

[37] A. Sarı, C. Alkan, and C. Bilgin, "Micro/nano encapsulation of some paraffin eutectic mixtures with poly(methyl methacrylate) shell: Preparation, characterization and latent heat thermal energy storage properties," *Applied Energy,* vol. 136, pp. 217-227, 2014/12/31/ 2014, doi: https://doi.org/10.1016/j.apenergy.2014.09.047.

[38] D. Yin, L. Ma, J. Liu, and Q. Zhang, "Pickering emulsion: A novel template for microencapsulated phase change materials with polymer–silica hybrid shell," *Energy,* vol. 64, pp. 575-581, 2014/01/01/ 2014, doi: https://doi.org/10.1016/j.energy.2013.10.004.

[39] S. Yu, X. Wang, and D. Wu, "Microencapsulation of n-octadecane phase change material with calcium carbonate shell for enhancement of thermal conductivity and serving durability: Synthesis, microstructure, and performance evaluation," *Applied Energy,* vol.

114, pp. 632-643, 2014/02/01/ 2014, doi: https://doi.org/10.1016/j.apenergy.2013.10.029.

[40] J. Giro-Paloma, G. Oncins, C. Barreneche, M. Martínez, A. I. Fernández, and L. F. Cabeza, "Physico-chemical and mechanical properties of microencapsulated phase change material," *Applied Energy,* vol. 109, pp. 441-448, 2013/09/01/ 2013, doi: https://doi.org/10.1016/j.apenergy.2012.11.007.

[41] L. Zhu, F. Dang, Y. Xue, K. Jiao, and W. Ding, "Multivariate analysis of effects of microencapsulated phase change materials on mechanical behaviors in light-weight aggregate concrete," *Journal of Building Engineering,* vol. 42, p. 102783, 2021/10/01/ 2021, doi: https://doi.org/10.1016/j.jobe.2021.102783.

[42] R. Illampas, I. Rigopoulos, and I. Ioannou, "Influence of microencapsulated Phase Change Materials (PCMs) on the properties of polymer modified cementitious repair mortar," *Journal of Building Engineering,* vol. 40, p. 102328, 2021/08/01/ 2021, doi: https://doi.org/10.1016/j.jobe.2021.102328.

[43] M. Hunger, A. G. Entrop, I. Mandilaras, H. J. H. Brouwers, and M. Founti, "The behavior of self-compacting concrete containing micro-encapsulated Phase Change Materials," *Cement and Concrete Composites,* vol. 31, no. 10, pp. 731-743, 2009/11/01/ 2009, doi: https://doi.org/10.1016/j.cemconcomp.2009.08.002.

[44] A. G. Entrop, H. J. H. Brouwers, and A. H. M. E. Reinders, "Experimental research on the use of micro-encapsulated Phase Change Materials to store solar energy in concrete floors and to save energy in Dutch houses," *Solar Energy,* vol. 85, no. 5, pp. 1007-1020, 2011/05/01/ 2011, doi: https://doi.org/10.1016/j.solener.2011.02.017.

[45] H. Zhou and A. L. Brooks, "Thermal and mechanical properties of structural lightweight concrete containing lightweight aggregates and fly-ash cenospheres," *Construction and Building Materials,* vol. 198, pp. 512-526, 2019/02/20/ 2019, doi: https://doi.org/10.1016/j.conbuildmat.2018.11.074.

[46] R. Parameshwaran, R. Naresh, V. V. Ram, and P. V. Srinivas, "Microencapsulated bio-based phase change material-micro concrete composite for thermal energy storage," *Journal of Building Engineering,* vol. 39, p. 102247, 2021/07/01/ 2021, doi: https://doi.org/10.1016/j.jobe.2021.102247.

[47] P. Aghdasi, I. D. Williams, B. Salazar, N. Panditi, H. K. Taylor, and C. P. Ostertag, "An Octet-Truss Engineered Concrete (OTEC) for lightweight structures," *Composite Structures,* vol. 207, pp. 373-384, 2019/01/01/ 2019, doi: https://doi.org/10.1016/j.compstruct.2018.09.011.

[48] J. Lei, J. Yang, and E.-H. Yang, "Energy performance of building envelopes integrated with phase change materials for cooling load reduction in tropical Singapore," *Applied Energy,* vol. 162, pp. 207-217, 2016/01/15/ 2016, doi: https://doi.org/10.1016/j.apenergy.2015.10.031.

[49] J. Lei, K. Kumarasamy, K. T. Zingre, J. Yang, M. P. Wan, and E.-H. Yang, "Cool colored coating and phase change materials as complementary cooling strategies for building cooling load reduction in tropics," *Applied Energy,* vol. 190, pp. 57-63, 2017/03/15/ 2017, doi: https://doi.org/10.1016/j.apenergy.2016.12.114.

[50] S. A. Memon, H. Z. Cui, H. Zhang, and F. Xing, "Utilization of macro encapsulated phase change materials for the development of thermal energy storage and structural lightweight aggregate concrete," *Applied Energy,* vol. 139, pp. 43-55, 2015/02/01/ 2015, doi: https://doi.org/10.1016/j.apenergy.2014.11.022.

[51] X. Bao *et al.*, "Development of high performance PCM cement composites for passive solar buildings," *Energy and Buildings,* vol. 194, pp. 33-45, 2019/07/01/ 2019, doi: https://doi.org/10.1016/j.enbuild.2019.04.011.

[52] A. Hassan, A.-H. I. Mourad, Y. Rashid, N. Ismail, and M. S. Laghari, "Thermal and Structural Performance of Geopolymer Concrete Containing Phase Change Material Encapsulated in Expanded Clay," *Energy and Buildings,* 2019/03/02/ 2019, doi: https://doi.org/10.1016/j.enbuild.2019.03.005.

[53] M. Li, Z. Wu, and J. Tan, "Heat storage properties of the cement mortar incorporated with composite phase change material," *Applied Energy,* vol. 103, pp. 393-399, 2013/03/01/ 2013, doi: https://doi.org/10.1016/j.apenergy.2012.09.057.

[54] M. L. V. Ramires, C. A. Nieto de Castro, Y. Nagasaka, A. Nagashima, M. J. Assael, and W. A. Wakeham, "Standard Reference Data for the Thermal Conductivity of Water," *Journal of Physical and Chemical Reference Data,* vol. 24, no. 3, pp. 1377-1381, 1995/05/01 1995, doi: 10.1063/1.555963.

[55] D. P. Bentz, "Transient plane source measurements of the thermal properties of hydrating cement pastes," *Materials and Structures,* vol. 40, no. 10, p. 1073, 2007/01/23 2007, doi: 10.1617/s11527-006-9206-9.

[56] E. Robertson, "Thermal properties of rocks," *U.S. Geological Survey,* vol. 88, 1988.

[57] Spheretek, "Speretek Technical Data Sheet - Hollow ceramic microspheres."

[58] B. G. Compton, B. K. Post, C. E. Duty, L. Love, and V. Kunc, "Thermal analysis of additive manufacturing of large-scale thermoplastic polymer composites," *Additive Manufacturing,* vol. 17, pp. 77-86, 2017/10/01/ 2017, doi: https://doi.org/10.1016/j.addma.2017.07.006.

[59] R. W. C. C. F. a. J. W. Tara L. Cavalline, "Impact of Lightweight Aggregate on Concrete Thermal Properties," *ACI Materials Journal,* vol. 114, no. 6, 11/1/2017, doi: 10.14359/51701003.

[60] P. Shafigh, I. Asadi, and N. B. Mahyuddin, "Concrete as a thermal mass material for building applications - A review," *Journal of Building Engineering,* vol. 19, pp. 14-25, 2018/09/01/ 2018, doi: https://doi.org/10.1016/j.jobe.2018.04.021.

[61] S.-C. Ng, K.-S. Low, and N.-H. Tioh, "Newspaper sandwiched aerated lightweight concrete wall panels—Thermal inertia, transient thermal behavior and surface temperature prediction," *Energy and Buildings,* vol. 43, no. 7, pp. 1636-1645, 2011/07/01/ 2011, doi: https://doi.org/10.1016/j.enbuild.2011.03.007.

[62] Y. Qin, "Pavement surface maximum temperature increases linearly with solar absorption and reciprocal thermal inertial," *International Journal of Heat and Mass Transfer,* vol. 97, pp. 391-399, 2016/06/01/ 2016, doi: https://doi.org/10.1016/j.ijheatmasstransfer.2016.02.032.

[63] J. Gui, E. Phelan Patrick, E. Kaloush Kamil, and S. Golden Jay, "Impact of Pavement Thermophysical Properties on Surface Temperatures," *Journal of Materials in Civil Engineering,* vol. 19, no. 8, pp. 683-690, 2007/08/01 2007, doi: 10.1061/(ASCE)0899-1561(2007)19:8(683).